Electronic supplementary information

Discriminating Active Sites for the Electrochemical Synthesis of H$_2$O$_2$ by Molecular Functionalisation of Carbon Nanotubes

Juyeon Lee,[a] Yesol Lee,[a] June Sung Lim,[b] Sun Woo Kim,[a] Hongje Jang,[a] Bora Seo,[c,d] Sang Hoon Joo,[b] and Young Jin Sa*[a]

[a]Department of Chemistry, Kwangwoon University, Seoul 01897, Republic of Korea.

[b]Department of Chemistry, Ulsan National Institute of Science and Technology (UNIST), Ulsan 44919, Republic of Korea.

[c]Hydrogen and Fuel Cell Research Center, Korea Institute of Science and Technology (KIST), Seoul 02792, Republic of Korea.

[d]Division of Energy & Environment Technology, KIST School, University of Science and Technology (UST), Seoul, Republic of Korea.

Corresponding author

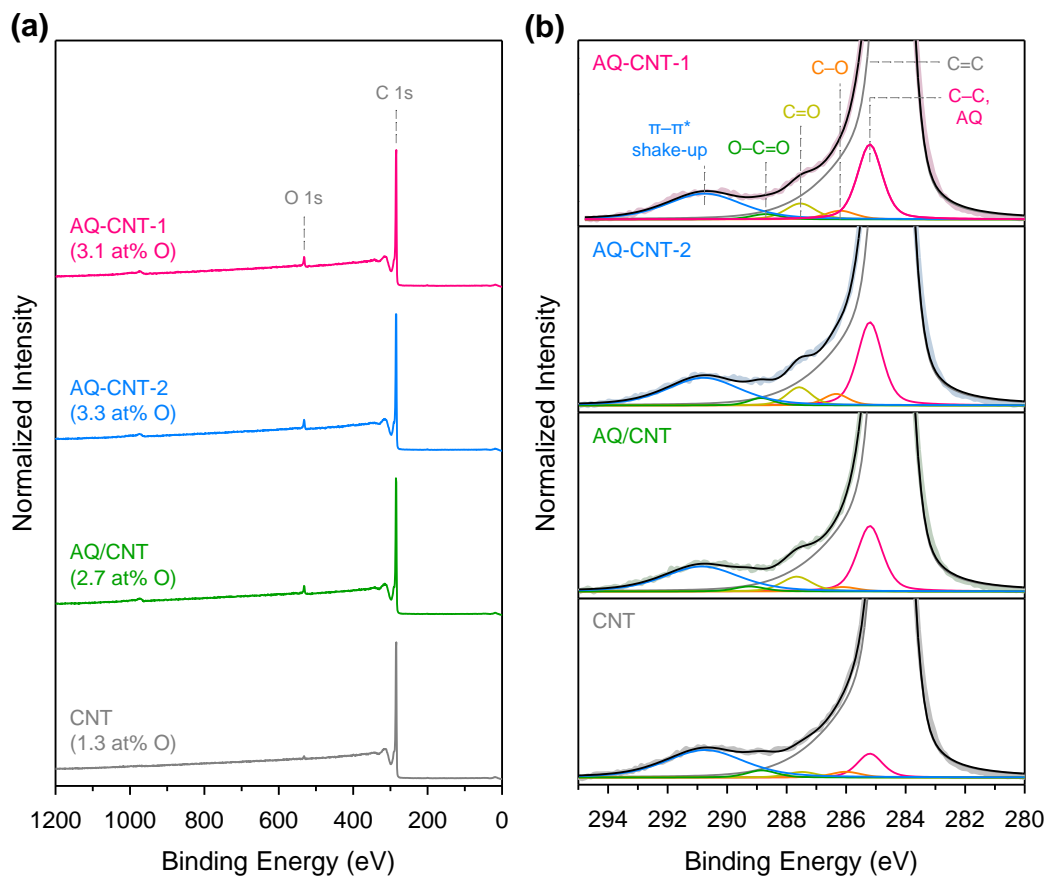*E-mail: youngjinsa@kw.ac.kr (Y.J.S.)

Table of contents

Fig. S1 C 1s XPS spectra and deconvoluted peaks of the AQ-CNTs, AQ/CNT, and bare CNT.

Table S1. Contents of C, O, and H in the catalysts obtained from combustion elemental analysis

Catalyst	C (wt%)	O (wt%)	H (wt%)
AQ-CNT-1	95.5	2.2	0.5
AQ-CNT-2	94.9	2.4	0.6
AQ/CNT	96.0	2.1	0.4
BA-CNT	96.1	1.4	0.8
Ph-CNT	96.7	0.8	0.5
CNT	97.5	0.4	0

Table S2. Relative peak areas obtained from deconvolution of C 1s XPS spectra of the AQ-CNTs, AQ/CNT, and bare CNT.

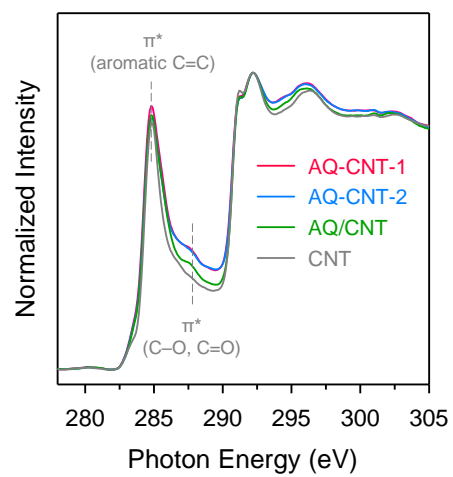| Catalyst	C=C (%)	C–C, AQ (%)	C–O (%)	C=O (%)	O–C=O (%)	π–π* (%)
AQ-CNT-1	82.4	6.9	1.0	1.8	0.6	7.3
AQ-CNT-2	81.5	7.6	1.1	1.8	0.7	7.3
AQ/CNT	84.1	6.2	0.5	1.7	0.6	7.0
CNT	87.5	2.3	0.6	0.6	0.8	8.1

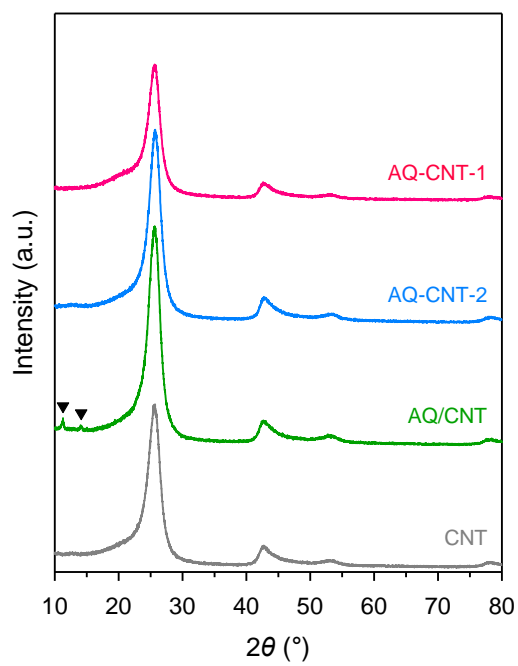**Fig. S2** C *K*-edge NEXAFS spectra of AQ-CNTs, AQ/CNT, and CNT.

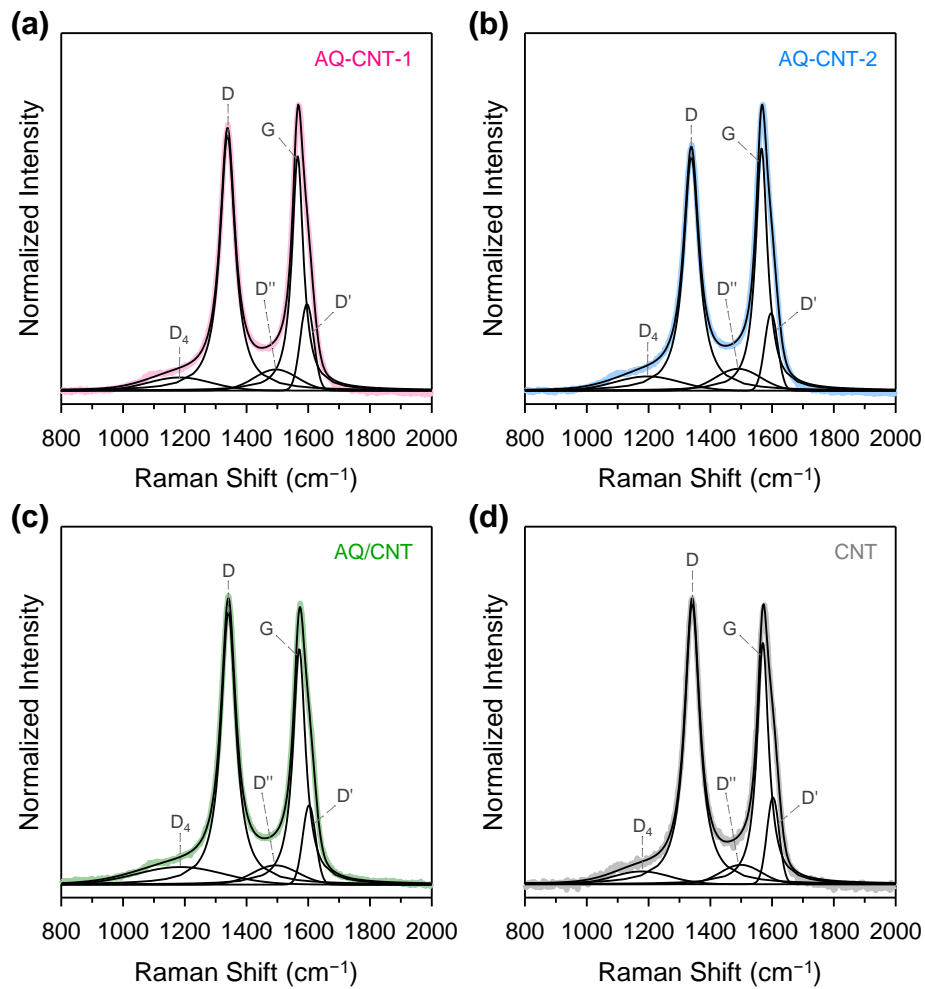**Fig. S3** XRD patterns of AQ-CNTs, AQ/CNT, and CNT.

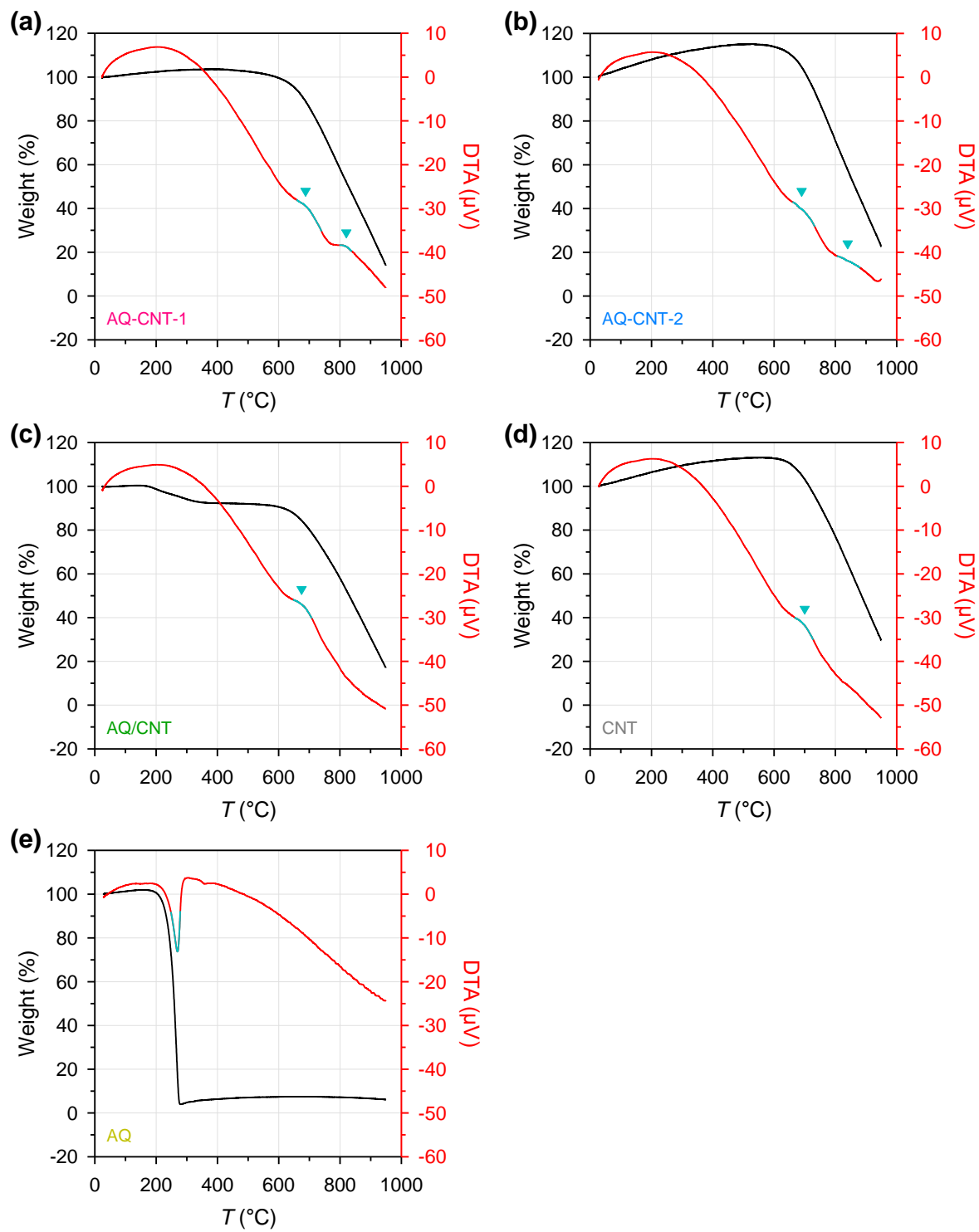**Fig. S4** Raman spectra and deconvoluted peaks for (a) AQ-CNT-1, (b) AQ-CNT-2, (c) AQ/CNT, and (d) CNT.

Fig. S5 TGA/DTA curves of (a) AQ-CNT-1, (b) AQ-CNT-2, (c) AQ/CNT, (d) CNT, and (e) AQ measured at a temperature ramping rate of 10 °C min^{-1} under Ar flow.
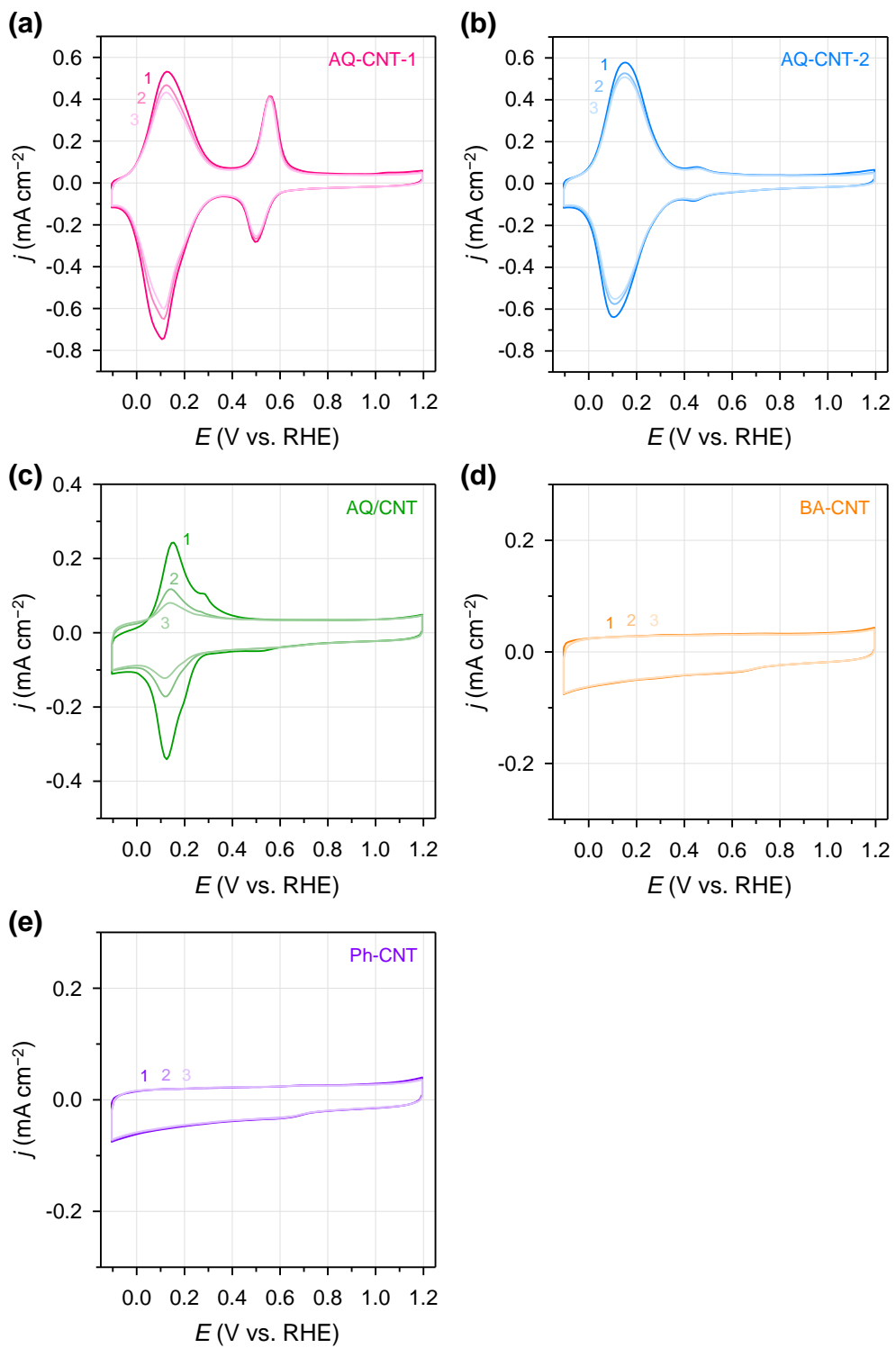
Fig. S6 CV curves of (a) AQ-CNT-1, (b) AQ-CNT-2, (c) AQ/CNT, (d) BA-CNT, and (e) Ph-CNT recorded consecutively three times.
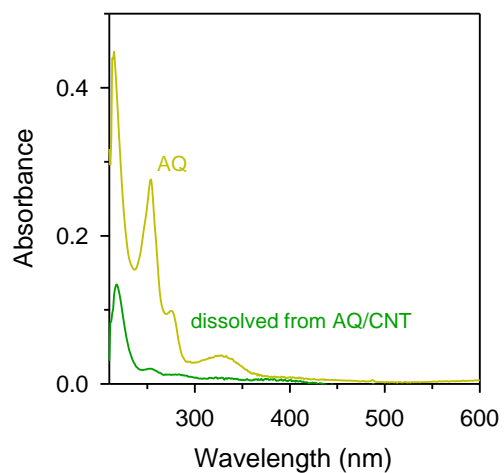
Fig. S7 UV-vis spectrum of 0.1 M KOH electrolyte after 100 potential cycles were applied to AQ/CNT. Prior to measurement, the used electrolyte was mixed with 25 volume% of acetonitrile. As a reference, the UV-vis spectrum of 0.1 mM AQ solution in 0.1 M KOH/acetonitrile (3:1 in volume).
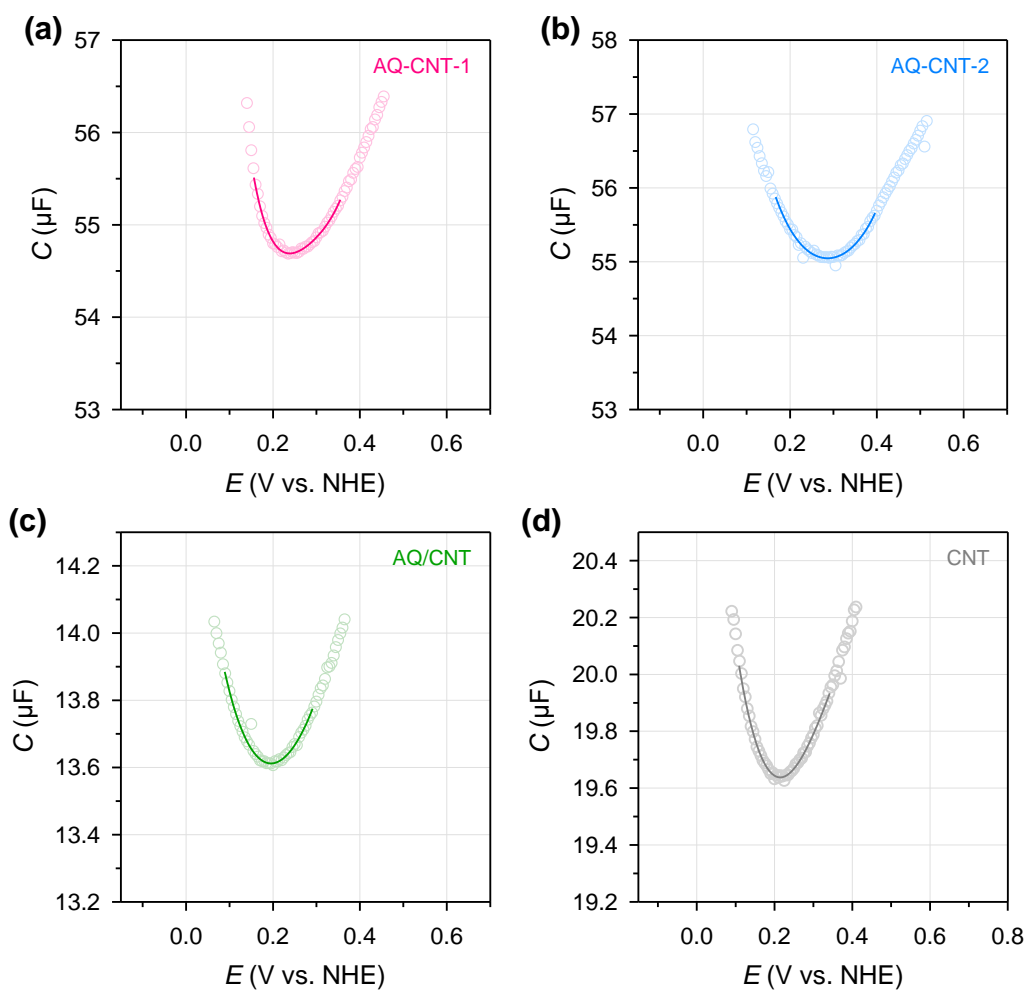
Fig. S8 Differential capacitance of (a) AQ-CNT-1, (b) AQ-CNT-2, (c) AQ/CNT, and (d) CNT measured in N_2-saturated 10 mM NaF.

Table S3. Potential of zero charge (PZC) and capacitance at the PZC of the AQ-CNT-1, AQ-CNT-2, AQ/CNT, and CNT determined from differential capacitance measurements.

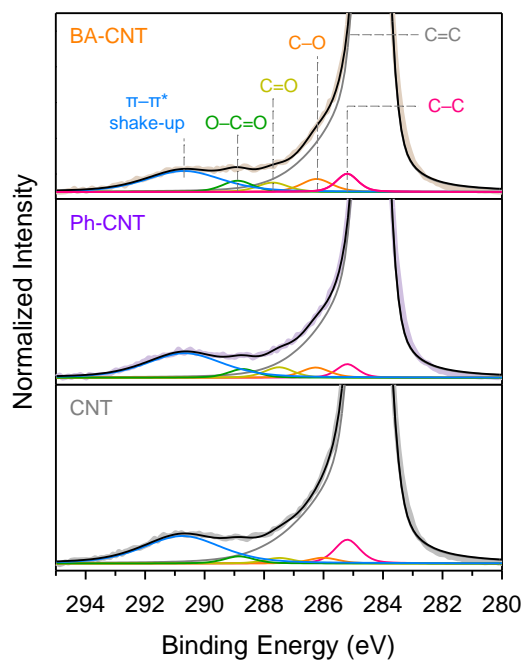| Catalyst	PZC (V vs. NHE)	C_{PZC} (µF)
AQ-CNT-1	0.24 ± 0.01	55 ± 3
AQ-CNT-2	0.28 ± 0.01	55 ± 13
AQ/CNT	0.20 ± 0.02	14 ± 6
CNT	0.22 ± 0.03	20 ± 6

Fig. S9 Deconvoluted C 1s XPS spectra of the BA-CNT, Ph-CNT, and bare CNT.

Table S4. Relative peak areas obtained from deconvolution of C 1s XPS spectra of the BA-CNT, Ph-CNT, and bare CNT.

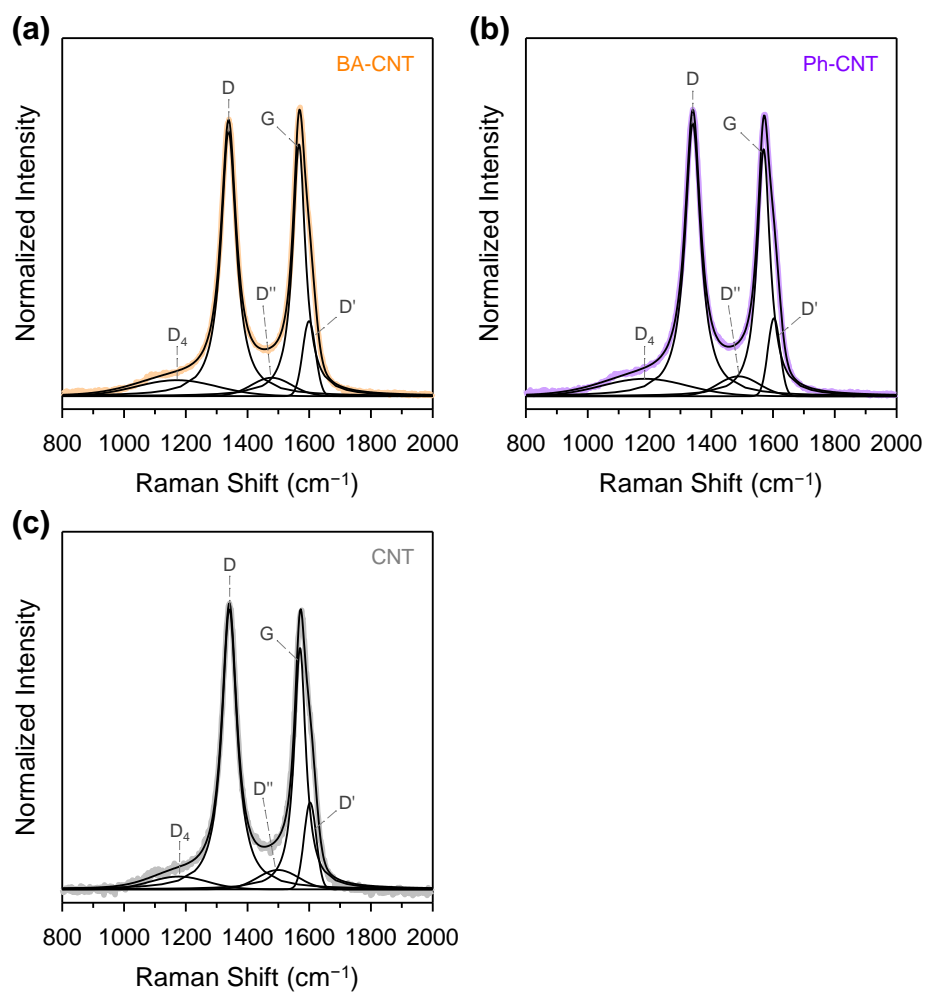| Catalyst	C=C (%)	C–C, AQ (%)	C–O (%)	C=O (%)	O–C=O (%)	π–π* (%)
BA-CNT	86.8	1.7	1.7	1.3	1.5	7.0
Ph-CNT	86.7	1.3	1.3	1.3	1.1	8.2
CNT	87.5	2.3	0.6	0.6	0.8	8.1

Fig. S10 Raman spectra and deconvoluted peaks for (a) BA-CNT, (b) Ph-CNT, and (c) CNT.
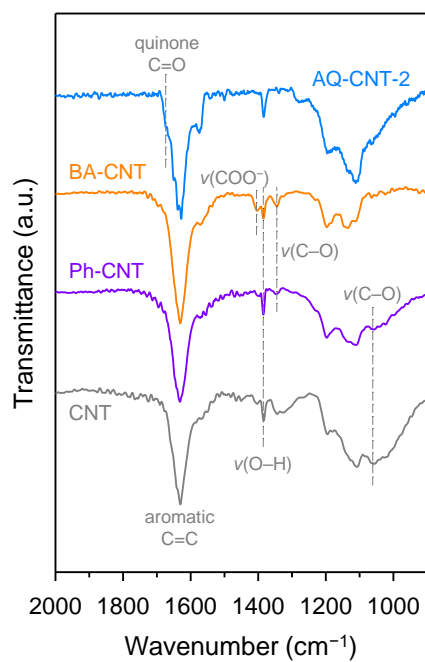
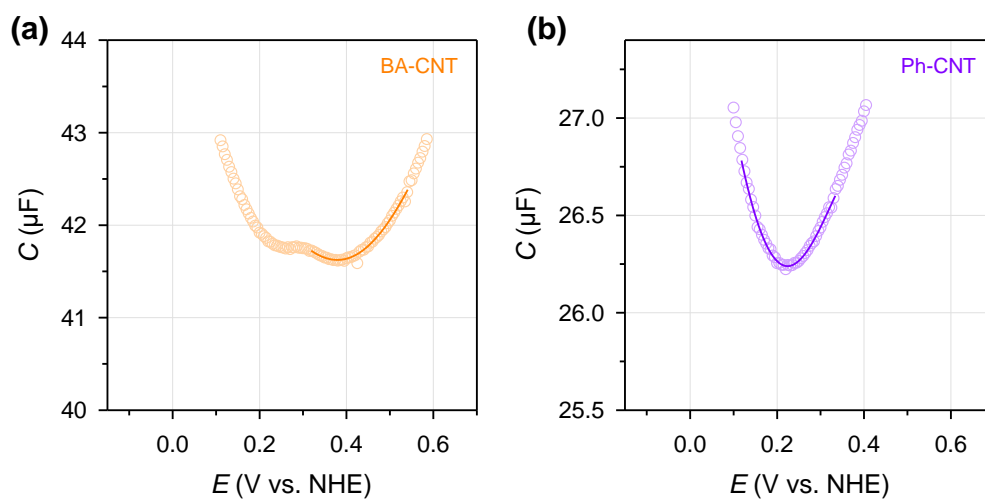**Fig. S11** FT-IR spectra of the AQ-CNT-2, BA-CNT, Ph-CNT, and CNT.

Fig. S12 Differential capacitance of (a) BA-CNT and (b) Ph-CNT measured in N_2-saturated 10 mM NaF.

Table S5. Potential of zero charge (PZC) and capacitance at the PZC of the BA-CNT and Ph-CNT determined from differential capacitance measurements.

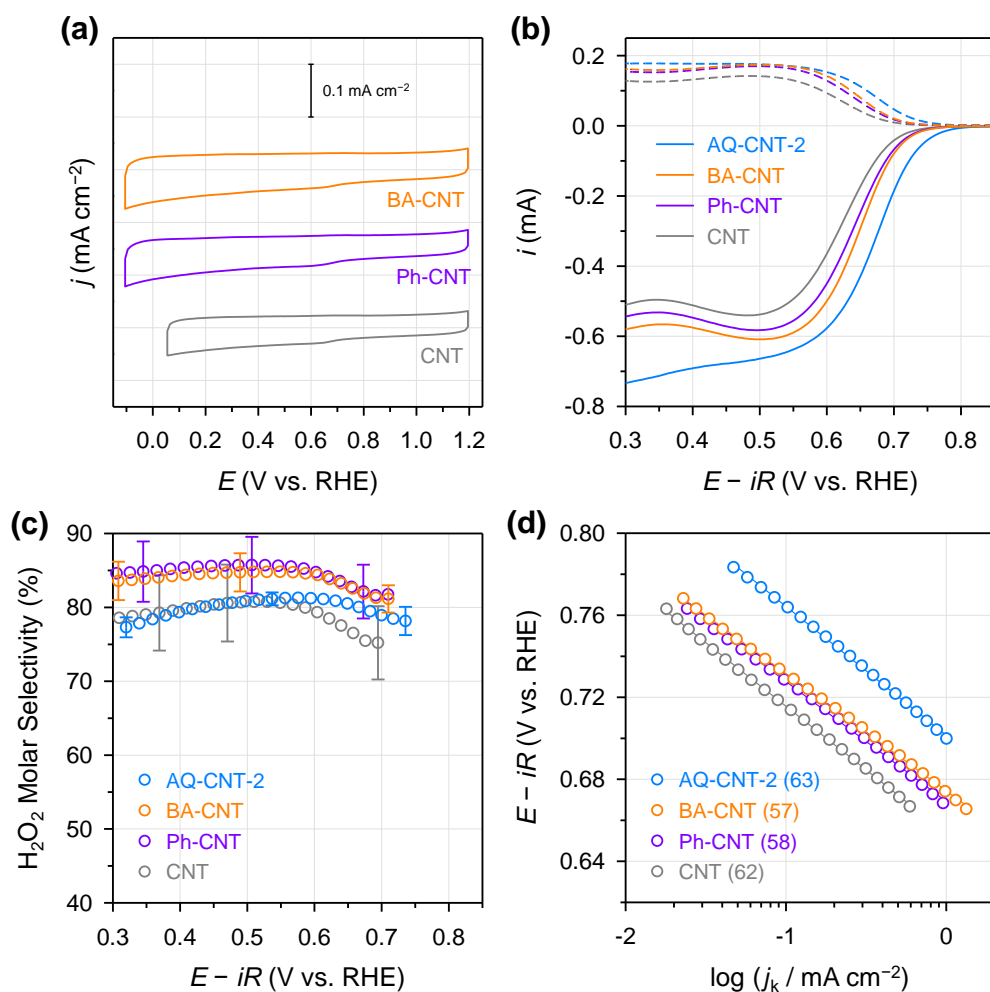| Catalyst	PZC (V vs. NHE)	C_{PZC} (μF)
BA-CNT	0.38 ± 0.01	42 ± 12
Ph-CNT	0.23 ± 0.01	26 ± 3

Fig. S13 (a) CV curves of the BA-CNT, Ph-CNT, and CNT measured in N_2-saturated 0.1 M KOH. (b) Linear sweep voltammograms of the BA-CNT, Ph-CNT, and CNT measured in O_2-saturated 0.1 M KOH using the RRDE method at an electrode rotation speed of 1600 rpm. (c) H_2O_2 molar selectivity as a function of the applied potential calculated from the RRDE responses. (d) Tafel plot; the numbers in the parenthesis indicate the Tafel slope (in mV dec^{-1}).
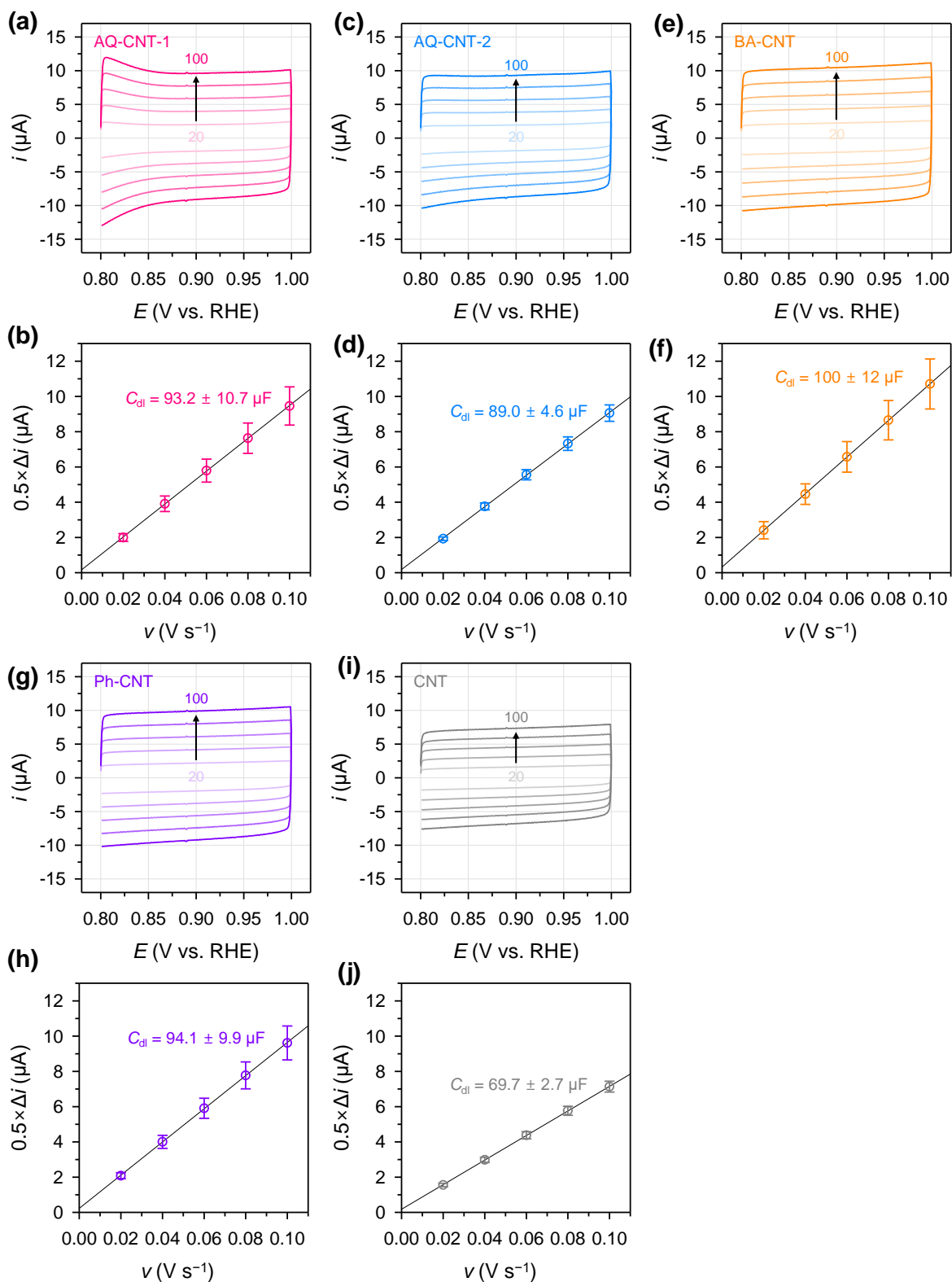
Fig. S14 CV curves of (a) AQ-CNT-1, (c) AQ-CNT-2, (e) BA-CNT, (g) Ph-CNT, and (i) CNT recorded at different scan rates (in mV s^{-1}) as indicated by the numbers in the plots in N$_2$-saturated 0.1 M KOH. Non-faradaic currents as a function of the scan rate (b) AQ-CNT-1, (d) AQ-CNT-2, (f) BA-CNT, (h) Ph-CNT, and (j) CNT obtained from the CV measurements.
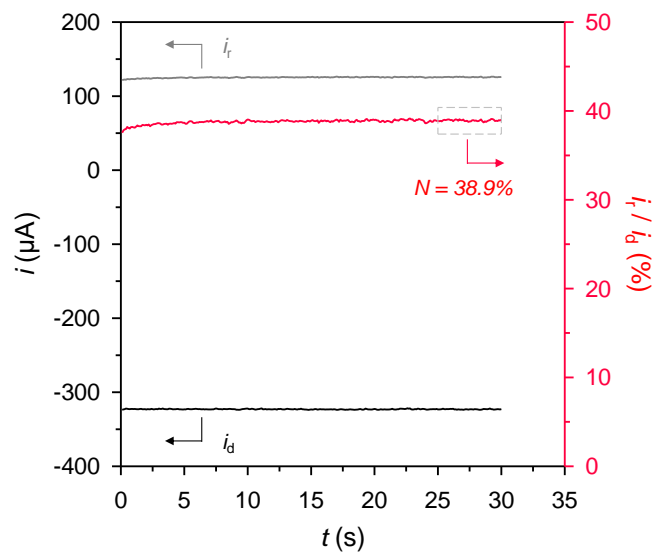
Fig. S15 Chronoamperometry measured in 2 mM K$_3$[Fe(CN)$_6$] + 0.1 M KOH with the electrode rotation speed of 1600 rpm at applied disk and ring potentials of −0.3 and 0.5 V (vs. Ag/AgCl), respectively, for determination of collection efficiency. (J. Lee, J. S. Lim, G. Yim, H. Jang, S. H. Joo, and Y. J. Sa, *ACS Appl. Mater. Interfaces,* 2021, **13**, 59904–59914.)